High Strength Thermoplastic Bonding for Multi-channel, Multi-layer Lab-on-Chip Devices for Ocean and Environmental applications

Sun, D., Tweedie, M., Gajula, D. R., Ward, B., & Maguire, P. D. (2015). High Strength Thermoplastic Bonding for Multi-channel, Multi-layer Lab-on-Chip Devices for Ocean and Environmental applications. Microfluidics and Nanofluidics, 19(4), 913-922. DOI: 10.1007/s10404-015-1620-2

Published in:
Microfluidics and Nanofluidics

Document Version:
Peer reviewed version

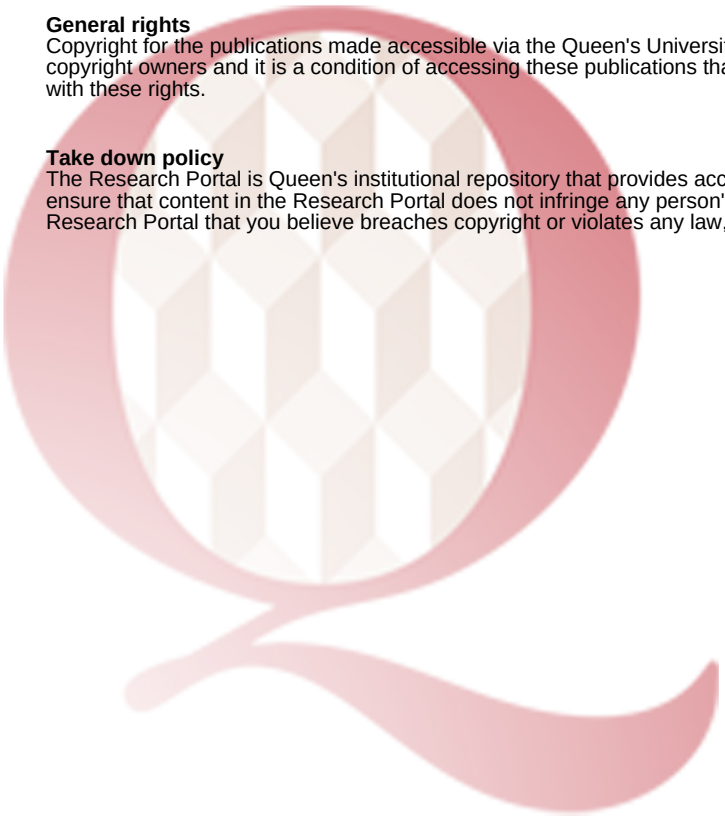

High Strength Thermoplastic Bonding for Multi-channel, Multi-layer Lab-on-Chip Devices for Ocean and Environmental applications

D. Sun*[a], M. Tweedie[b], D. R. Gajula[c], B. Ward[d], P.D. Maguire[b]

[a] School of Mechanical and Aerospace Engineering, Queen's University Belfast, Belfast BT9 5AH, United Kingdom. Email: d.sun@qub.ac.uk; Fax: +44 28 90974148; Tel: +44 28 90974701
[b] Nanotechnology and Integrated Bio-Engineering Centre (NIBEC), University of Ulster, Newtownabbey BT37 0QB, United Kingdom
[c] School of Electronics, Electrical Engineering and Computer Science, Queen's University Belfast, Belfast BT9 5AH, United Kingdom
[d] School of Physics and Ryan Institute, National University of Ireland, Galway, Ireland

Abstract

A solvent-vapour thermoplastic bonding process is reported which provides high strength bonding of PMMA over a large area for multi-channel and multi-layer microfluidic devices with shallow high resolution channel features. The bond process utilises a low temperature vacuum thermal fusion step with prior exposure of the substrate to chloroform ($CHCl_3$) vapour to reduce bond temperature to below the PMMA glass transition temperature. Peak tensile and shear bond strengths greater than 3 MPa were achieved for a typical channel depth reduction of 25 µm. The device-equivalent bond performance was evaluated for multiple layers and high resolution channel features using double-side and single-side exposure of the bonding pieces. A single-sided exposure process was achieved which is suited to multi-layer bonding with channel alignment at the expense of greater depth loss and a reduction in peak bond strength. However, leak and burst tests demonstrate bond integrity up to at least 10 bar channel pressure over the full substrate area of 100 mm x 100 mm. The inclusion of metal tracks within the bond resulted in no loss of performance. The vertical wall integrity between channels was found to be compromised by solvent permeation for wall thicknesses of 100 µm which has implications for high resolution serpentine structures. Bond strength is reduced considerably for multi-layer patterned substrates where features on each layer are not aligned, despite the presence of an intermediate blank substrate. Overall a high performance bond process has been developed that has the potential to meet the stringent specifications for lab-on-chip deployment in harsh environmental conditions for applications such as deep ocean profiling.

Keywords: PMMA, Bonding, Ocean sensing, Lab-on-Chip

Introduction

Microfluidics, originally concerned with microanalysis, has expanded considerably in the last decade with much of the research effort focussed on lab-on-chip devices for medical diagnostics and blood analysis (Sackmann et al. 2014). Commercial components and systems are becoming available, particularly for gene sequencing and point of care diagnostics (Volpatti et al. 2014), although the commercialisation of low cost devices is still at an embryonic stage (Tomazelli et al. 2014). There is however a concern that the microfluidic platform technology, while technically superior to traditional methods, has enabled only iterative progress and has not delivered the breakthroughs in biomedical applications that were originally envisaged (Sackmann et al. 2014; Whitesides 2006). The successful adoption of microfluidic lab-on-chip technology will depend on its ability to deliver truly enabling functionality compared to traditional techniques and on overcoming barriers to commercialisation. These include component compatibility and integration into functional systems (Ducrée 2013) and matching the materials and fabrication processes to low cost / high throughput manufacturing requirements, e.g. using thermoplastics rather than elastomer materials (Volpatti et al. 2014).

Microfluidics for environmental monitoring, especially for continuous and autonomous chemical or biological analysis offers scope for such a breakthrough. Nevertheless, despite the early origins of

microfluidic technology in microanalysis, uptake here has been slower than expected. This reflects the major challenges in automating sample processing, developing detection methods and operating sensors reliably in the wild, unattended environment (Whitesides 2006). Monitoring marine conditions from coastal to deep ocean locations is now considered of critical importance. There is strong evidence that oceans play a key role in climate regulation (Field et al. 2014) and economic exploitation of the seas is expected to extend and intensify. Monitoring efforts to date have focussed on fresh water (Bridle et al. 2014) whereas the marine environment presents considerable additional challenges (Mills et al. 2012). Accessing remote locations, on-board ship analysis or sample transport to land is expensive, time-consuming, and can result in under-sampling and compromised sample integrity (Byrne 2014). It often fails to provide representative information over changes in time, whether short or long-term (Mills et al. 2012).

Although in-situ measurements are not yet routine, in-situ marine sensors have been in use for a number of years to measure physical parameters such as pH, conductivity and O_2 and sensor arrays are now available to measure multiple parameters simultaneously. The Alliance for Coastal Technologies (http://www.act-us.info/) provides a useful database of current instruments and deployment platforms. Miniaturisation of ocean instrumentation is a major focus of on-going research and the scope for microfluidics and lab-on-chip devices would appear obvious. However the very demanding specifications for accuracy and stability and the considerable fabrication challenges have presented a near insurmountable barrier to progress. Hence research in this area is still in its infancy. Examples to date include chemical sensors (Provin et al. 2013), autonomous analytical devices for high spatial and temporal resolution (Legiret et al. 2013; Rérolle et al. 2013; Xi et al. 2011), on-chip electrochemical microsystems (Herzog et al. 2013) and microbial ecology devices (Rusconi et al. 2014; Seymour et al. 2010).

Using lab-on-chip approaches to successfully tackle specific measurement problems where essentially no alternative techniques are available, would establish the principle and provide a route to more widespread adoption. As an example of such an application, we are interested in the ocean CO_2 system which is of fundamental importance to contemporary studies of seawater chemistry yet continues to be chronically under-sampled in both space and time. Very large uncertainties in this budget still remain, despite the history of CO_2 ocean observations for the last several decades (for example the SOCAT atlas lists over 7 million ship borne underway ocean CO_2 measurements, http://www.socat.info/about.html). Current CO_2 observations are almost exclusively limited to the surface and use large sensors attached to expensive research vessels (Byrne et al. 2014). We have demonstrated autonomous profiling of microstructure oceanic variables at the surface (e.g. dissipation rate of turbulent kinetic energy, temperature, conductivity) (Ward et al. 2014; Sutherland et al. 2013), density-driven length scales (Sutherland et al. 2014) and surface forcing (Callaghan et al. 2014). However an autonomous system for vertical profiling and CO_2 analysis would need to capture and store multiple seawater samples, allow for extended analysis time, be scalable for deployment on the existing float network, and operate reliably and accurately over an extended time (~ years) with large pressure changes and temperature cycling. Such a system can only be realised through microfluidics. At the outset, this poses a considerable challenge for materials, fabrication, sealing and reliability testing at each stage. In this work, we investigate the development of a robust microfluidic platform for ocean deployment and focus on thermoplastic fabrication and sealing to this end. While this topic has been explored to a degree in the past, the specific reliability and design requirements for marine devices, e.g. large area bonding, high resolution multi-channel and multiple patterned layers, deserve detailed investigation (Temiz et al. 2015).

Materials such as silicon and glass are brittle and require complex fabrication processes especially for output connections. PDMS is currently the dominant alternative material but issues such as porosity, chemical resilience (Ogilvie et al. 2011) and ultimately manufacturability (Sackmann et al. 2014) mean that thermoplastic alternatives e.g. PMMA or COC, will be required. These are cost-effective, suitable for mass production yet retain the relative ease of prototyping. There is evidence that PMMA offers better resistance against biofouling which can be a major problem for long-term deployment of sensors in the marine environment (Alexandra et al. 2013). Thermoplastic sealing has received attention for microfluidic devices (Tsao et al. 2009) via direct fusion bonding (above the polymer glass transition temperature, T_g) as well as with alternative treatments such as ultrasonics (Zhang et al. 2010; Li et al. 2009), plasma (Brown et al. 2006; Kettner et al. 2006; Awaja et al. 2011), UV (Tsao et al. 2007; Shinohara et al. 2011) and solvent-assisted bonding (Brown et al. 2006) to limit heat and pressure induced feature deformation. The latter approach has been reported for a number of polymer – solvent combinations, e.g. temperature-

activated isopropyl alcohol (Ng et al. 2008) or ethanol (Rahbar et al. 2010), 1,2-dichloroethane/ethanol at room-temperature (Lin et al. 2007), dimethyl sulfoxide /H_2O/methanol (Brown et al. 2006), decalin-ethanol COC (Wallow et al. 2007), $CHCl_3$ (De Marco et al. 2013; Ogilvie et al. 2010) , ethanol with UV (Tran et al. 2013) and where the solvent interaction is obtained via immersion or vapour exposure. High strength bonding is achievable by these processes at temperatures sufficiently low to minimise temperature-induced channel deformation. Nevertheless polymer surface dissolution and softening may also lead to dimensional change or distortion (Uba et al. 2015).

Materials and methods

PMMA samples (Cut Plastics Ltd, Devon UK, average molecular weight 2.5 – 3.0 x 10^6 g mol^{-1}) 15 mm x 15 mm x 3 mm for bond tensile, 10mm x 100mmx 3 mm for shear tests and 100 mm x 100 mm x 10 mm for pressure/leak tests and microscopy were used. Substrates were milled back to obtain a flat surface prior to patterning or bonding. Thermal fusion bonding was also carried out without pre-treatment in an EVG (EVG 520HE) bonder for temperatures and pressures in the range 100 ºC – 135 ºC and 100 – 200 Ncm^{-2}, respectively. The heat was applied and the chamber evacuated until the temperature on both bonding plates had stabilised (~20 min). Thereafter the pressure was applied for a number of minutes. For plasma pre-treated samples, RF vacuum plasma exposure was carried out in O_2 at 10 mTorr in an inductively coupled plasma system, details of this system are provided elsewhere (Baby et al. 2011). The system was operated at low RF power (100W, 13.56 MHz) to ensure low surface bombardment energy. An additional substrate bias (0 – 80W, 10MHz) allowed adjustment of the bombardment energy without affecting plasma conditions. $CHCl_3$ pre-treatment was achieved by exposing samples to $CHCl_3$ (Sigma-Aldrich) vapour under atmospheric pressure at 20 ºC in a container with lid, for various exposure times (2 – 20 min) at an offset distance of 4mm. After pre-treatment, samples were either contact bonded in air or under vacuum (0.15 mBar) in the EVG bonder. The transfer time to the bonder was < 1 min, and the system was evacuated for 1 min followed by application of heat and pressure until conditions stabilised at 80 ºC and 175 Ncm^{-2}, to avoid removal of the surface $CHCl_3$. Confocal Raman spectroscopy was carried out to estimate the evolution of surface $CHCl_3$ content using a LabRam 300 (Horiba Jobin Yvon), at 632.81 nm. The $CHCl_3$ peak amplitude variation at 669 cm^{-1} (Rothschild et al. 1965) was chosen to avoid PMMA background interference. The $CHCl_3$ depth profile was estimated by adjusting the focus optics. For tensile testing, the bonded samples were attached to 20 mm long PMMA extension substrates using epoxy, before fitting to the gripper of the Instron 3344 tensile tester. The cross head speed was 0.5 mm/min and the bonding area was 15 mm x 15 mm. Channels were milled into substrates with different patterns for high pressure - leak tests with initial dimensions in the range 150 -1000 µm (width) and 200-500 µm (height). Dimensional changes in the milled channels due to bonding were observed using optical microscopy and SEM (Joel 6500). In order to explore the sensitivity of potential devices structures to bonding processes, a number of multilayer stacks with different patterns were bonded and pressure-leak tested. Also thin (50 nm) metal tracks were sputtered onto PMMA and subsequently bonded to patterned sheets. These were leak tested to investigate the potential for microscopic weakness at the PMMA bond – channel - metal interfaces which might allow leakage between neighbouring channels

Design Considerations and Storage Manifold

In Fig. 1 we show an ocean chemical analysis sub-system as an example device for considering bond requirements and performance. The final system will feature a number of such components integrated together to measure CO_2 (dissolved inorganic carbon) depth profiles via flow injection analysis principles (Hall et al. 1992; Plant et al. 2009). The sub-system in question comprises multiple sample capture and storage cells on a PMMA manifold along with multiplexed reagent metering and mixing. This will be based on discrete high pressure ocean solenoid valves (Lee Products Ltd), Fig. 1 (c), since current hydraulic microfluidic valves cannot deliver valve performance nor meet the chemical, reliability and power constraints of the proposed application. The multiplexed architecture will help maintain the valve count to ~1 per channel with a total of two pumps but this will impact on channel design requirements. The overall manifold footprint is constrained by the available space on existing ocean floats (Argo, http://www.argo.ucsd.edu/) and by fabrication equipment limitations to approximately 100 mm x 100 mm. Channel dimensions and tolerances are constrained by the flow resistance required to achieve the required sample capture speed for depth resolution yet need to account for microvalve footprint, on-board reagent

payload volume, uniform reagent metering and the potential for inter-channel cross-diffusion inherent in the proposed architecture. Integration of all components will require manifold devices of 5 – 7 layers and associated bonding. The majority of these layers will be patterned with channels and features. Ultimate deployment in the deep ocean will demand demonstrably robust and reliable devices capable of lasting a number of years, unattended and exposed to challenging environmental conditions including high pressure variations to profile from the surface to ~2000 m.

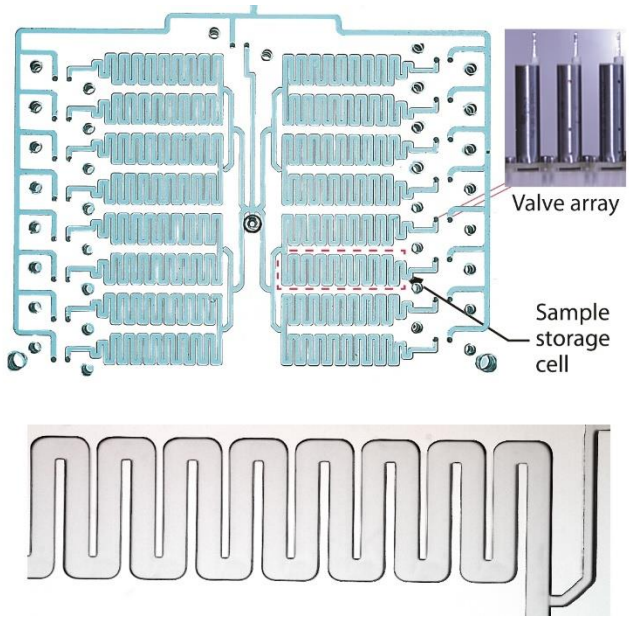

Fig.1 Figure 1: Image (colour enhanced) of 100mm x 100mm bonded PMMA - PMMA manifold comprising 16 (2 x 8) sample and hold storage cells, with one valve per cell.

By comparison with other plastic lab-on-chip devices, the development of a lab-on-chip ocean chemical profiling system will require specific consideration of large area uniform bonding of multiple patterned layers; high density and long channels; tight depth uniformity to avoid species trapping and flow resistance variation; chemical resilience. The presence of invisible microbubbles of trapped air in the inter-channel regions after bonding would normally not be an issue but with lifetime high pressure cycling this could lead to fatigue points. Given the difficulty and cost of ocean field testing, extensive laboratory testing will be needed to simulate environmental conditions as best as possible. While the proposed device will need to operate at high ambient pressures (~200 bar), the differential pressure on any channel is expected to be moderate ($\leq$ 1 bar). The required bond strength however will be difficult to determine except by trial and error. We therefore aim for the maximum bond strength achievable with due consideration for other design factors particularly channel dimensional integrity. Measurements of bond strengths by a number of techniques have been reported and have provided indications of relative performance between different process options without necessarily providing an absolute determination of suitability for a particular application. Nevertheless, in this paper, we follow such measurement protocols as reported in the literature as well as developing additional test protocols of particular relevance to the design issues outlined above. We have investigated thermal fusion bonding as well as plasma pre-treatment. However the main focus of the paper is on solvent vapour assisted bonding. The flow characterisation and functional operation of this and other sub-components will be reported in the near future.

Results

Vacuum thermal fusion bonding, near the glass transition temperature (T_g) of 105 ^oC, with 100 – 200 Ncm^{-1} applied pressure resulted in high strength bonds but also thermal reflow which affected channel dimensions and, in multi-layer stacks, caused a degree of misalignment of channels on different layers. Bonding below T_g resulted in poor or inconsistent bonding across the substrate area. Vacuum plasma pre-

treatment required an enhanced surface roughness of ~27 nm (R_a) compared to ~5 nm for untreated samples, achieved by ion bombardment at high substrate bias. Given the critical requirement for the device to withstand very high ambient pressures, the possibility of creating voids at the bond interface due to roughness/pitting must be avoided and therefore plasma pre-treatment was not pursued. Solvent treatment of PMMA is known to enhance channel smoothness. However to minimise the potential for long-term fatigue, direct contact with liquid was avoided and instead minimum solvent inclusion was achieved using vapour exposure. Measurement of milled channel roughness after solvent exposure was used as a preliminary screening test to determine optimal offset distances and temperature range. From this, a 4mm offset distance and a substrate temperature of 80 ^{o}C was chosen for subsequent tests for bond strength against time. The as-machined PMMA surface roughness is ~ 6um.Depending on the $CHCl_3$ treatment time (i.e. 2 min – 20 min), the surface roughness first decreases then increases, with the lowest surface roughness (~ 2 um) observed after 10 min. Although bond quality dependence on roughness at the nanoscale has been reported (Shao et al. 2006), in this case the vapour-induced softening occurs to a depth of 20 – 50 microns, i.e. much deeper than the original roughness due to milling and therefore minimises the potential dependence of bond strength on roughness.

Fig. 2 shows the effect of $CHCl_3$ vapour exposure time on the tensile and shear bonding strength of PMMA. With double-sided treatment, both pieces are exposed to solvent simultaneously for a given time, followed immediately by low pressure (manual) contact before thermal fusion bonding. Maximum tensile bond strengths of 3.5 – 4.0 MPa are obtained over a wide process window (4 – 12 min). After extended exposure (> 12 min) the bond strength deteriorates. For single-sided treatment, no significant bonding occurred until after 8 min exposure and the maximum bond strength was slightly lower than double-sided at 3 MPa after 15 min exposure. The lap shear strength has been reported for double-sided treated sample only, which also peaks at 12 min, similar to the tensile strength of the double-sided treated samples.

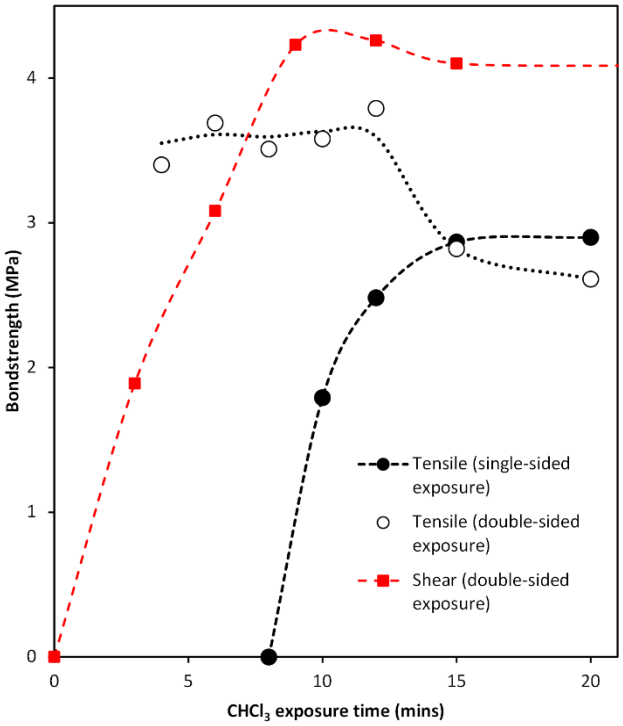

Fig. 2 Tensile bond strength for thermal fusion bonding of PMMA – PMMA with prior double-sided and single-sided vapour exposure and shear bond strength **for** double-side vapour exposure.

For larger area substrates, suitable for device fabrication, resting surface contact can lead to voids which are potential fatigue /failure points while press contact can impact on channel deformation. We evaluated this using a thin deformable PMMA membranes bonded to PMMA sheet where it was clear that even with pressure and temperature steps, voids once formed were difficult to dislodge. It was important therefore to avoid void formation at the very initial contact between solvent exposed pieces via the immediate application of sufficient (low) pressure uniformly across the bond area. For solid pieces this

was more readily achieved using a vacuum press. However the use of vacuum may also lead to outgassing of surface solvent and impact on bonding. The issue of solvent inclusion also needs to be considered as its impact on long term material strength and chemical outgassing into analyte is unknown. Immediately after solvent exposure, the solvent penetration depth was observed from iodine stain images, to be ~60 µm.

In Fig 3, the Raman peak at 669 cm^{-1} was used to estimate the $CHCl_3$ concentration with depth of single unbounded substrates for two starting conditions of (A1) 12 min in $CHCl_3$ vapour at 4 mm height followed by 60 min in vacuum at 80 °C with surface in contact with EVG bonder top plate, then 120 min cool down, and (B1) 12 min in $CHCl_3$ vapour at 4 mm height followed by 240 min in air at room temperature. Subsequent steps were (A2, B2) 17 hours in vacuum at room temperature, (A3, B3) 24 hours in vacuum at 80 °C and (A4, B4) 44 hours in air 80 °C. The initial $CHCl_3$ penetration depth is 10-20um, which increases after initial vacuum step A to approximately 30um along with a reduction in peak concentration at about 10µm below the surface. With the initial air step (B), some $CHCl_3$ is able to escape and the peak concentration is reduced without affecting the penetration depth significantly. For both cases (A, B), the greatest reduction in $CHCl_3$ content occurred after a long exposure to ambient. A subsequent vacuum with heat step displayed little further change. Overall it is clear that significant $CHCl_3$ is retained in the substrate after vacuum sequence A indicating that vacuum outgassing is limited by contact with the bonder top plate.

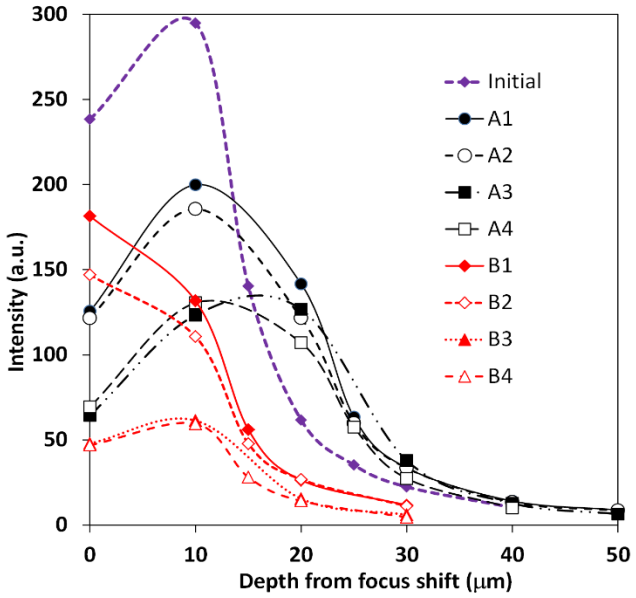

Fig. 3 $CHCl_3$ 669 cm^{-1} Raman peak height versus depth for 12 min exposure to $CHCl_3$ vapour at 4 mm height followed by exposure to air / vacuum at different temperatures. A1: 180 min in vacuum at 80 °C with surface in contact with EVG bonder top plate. B1: 240 min in air at room temperature. A2, B2: 17 hours in vacuum at room temperature. A3, B3: 24 hours in vacuum at 80 °C. A4, B4: 44 hours in air 80 °C. (Note A refers to samples with initial vacuum step and B refers to samples with initial air step, with the subsequent indicated treatments being consecutive on each piece).

In multi-layer structures multiple patterned layers can be expected with various degrees of alignment which may affect load transfer during the bonding process under pressure. Using a concurrent single-sided bond process (12 min exposure, 80 °C) to simultaneously bond two patterned layers (A and C) to an intervening blank (B), Fig. 4 (a), the impact on bond strength is observed to be clearly pattern sensitive and dependent on channel alignment. Where alignment is greatest, the maximum bond strength (2 MPa) is reduced by ~20% compared to the peak bond strength (2.5 MPa) for single patterned layer and decreases to ~0.1 MPa as the misalignment increases.

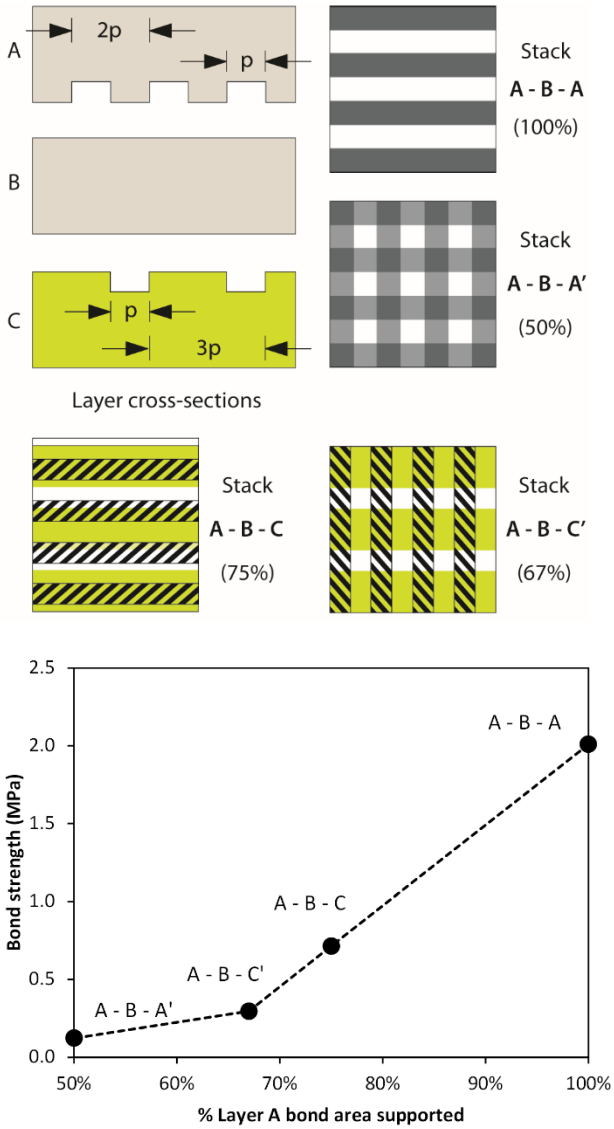

Fig. 4(a) Cross-sectional and plan views of patterned substrates A and C with different channel pitches for simultaneous bonding to blank substrate B. The half-pitch p = 0.5mm. A' and C' represent patterns A and C rotated by 90°. Percent figures indicate fraction of bond area on substrate A supported by substrate C, (b) tensile strength of multi-layer stacks versus supported bond area fraction. The failed surface is substrate A.

Micro-channels of various depth (50um, 100um, 200 um) were milled on PMMA surfaces which were then treated by $CHCl_3$ vapour for 12 min. In Fig. 5(a) the single-side bonded images indicate that channel deformation depends on whether the patterned or unpatterned side is exposed. The latter shows lid encroachment into the channel with a greater reduction in height (20%) and area (18%) compared to the exposure of the channelled substrate which suffers a 13% and 10% reduction in height and area respectively. With double-sided bonding the channel height reduction was ~25µm (14%), Fig. 5(b). Multi-layer bonding is also shown in Fig. 5(c). The deformation of the channel cross-section is due to the contact between a hard and a $CHCl_3$ softened interface under pressure whereas for the double-sided bond, both surfaces would be equally soft and deformation is minimal.

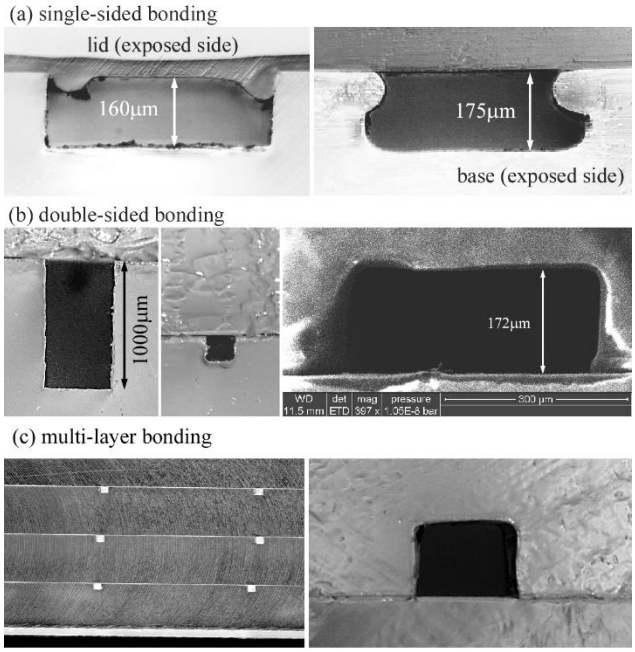

Fig. 5 Cross-sectional optical and SEM images of typical micro-channel before and after bonding, (a) single-sided bonding of 200 μm deep channels with either the unpatterned lid or the channel base exposed to vapour prior to bonding. (b) Double-sided bonding at 80°C, for an initial channel depth 200μm except where indicated (1000 μm). (c) An example of multi-layer bonding of substrates with 200 μm deep channel features.

Tensile tests are restricted to small area unpatterned pieces. To evaluate bond quality on large area (100 mm x 100 mm) device-standard patterned layers, a number of high pressure leak and burst tests were performed. All substrates obtained the standard 12 min $CHCl_3$ single-sided (unpatterned side) solvent exposure followed by EVG vacuum bonding at a substrate temperature of 80 °C and 175 Ncm^{-2} for 25 min. A number of serpentine channel patterns were created across the substrate with variable inter-channel spacing (W) from 0.1 mm to 10 mm, Fig. 6(a). After filling with liquid and sealing the channels at one end, the other end was attached to a high pressure nitrogen line. The pressure was increased in step (1 bar) and with a single-side bonded structure, and for wall thicknesses down to 100 μm, no deflection and no bond failure was observed. However for the double-side bonded structures, the top bond failed at low pressures for a wall thickness of 100 μm. In another leak test structure, thin (50 nm) Au metal tracks were deposited by DC sputtering onto a plain PMMA substrate which was subsequently bonded to a substrate with a spiral channel pattern of diameter 90 mm, Fig. 6(c, d). After liquid filling and sealing at one end, the channel was subjected to N_2 pressures up to 10 bar. Again, for pressures up to 10 bar, no leakage was observed at the metal – PMMA interface across the whole substrate, Fig. 6(d) hold (2 min) sequence up to 10 bar, maximum. At each hold stage, the bonded substrates were observed for inter-channel leakage. Across the full area of the substrate, no leakage was observed for the maximum pressure of 10 bar. With thin sidewalls, the possible flexing or bulging of the wall and its impact on bond integrity was investigated using a dual channel arrangement, Fig. 6(b) separated by a thin wall. One channel was pressurised with nitrogen and the liquid deflection in the adjacent channel provided an indication of wall bulging or deflection.

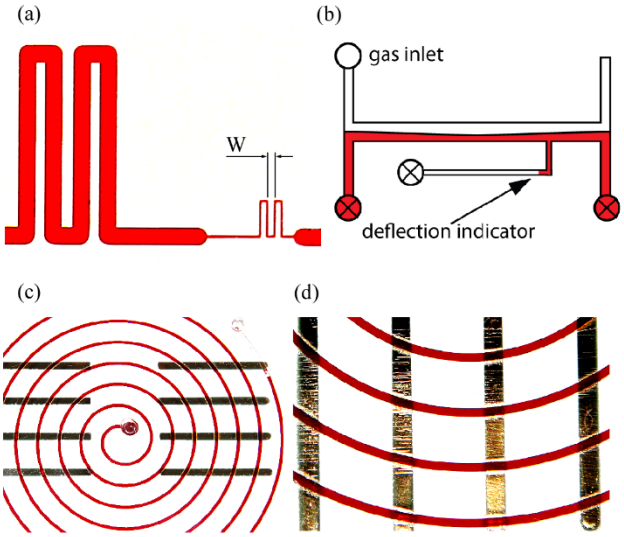

Fig. 6 (a) Test piece with serpentine channels with variable wall thickness (W) from 0.1 mm to 10 mm. (b) typical test structure for investigating thin inter-channel wall deflection and bond strength during pressure application. (c) test piece with spiral pattern and (d) gold electrode (1mm wide, 50 nm thick) after pressure limit test indicating no inter-channel leakage up to 10 bar.

Discussion

We have explored fusion bonding of 100 mm x 100 mm substrates across the pressure-temperature parameter space. Results were similar to the literature reports, namely maintaining feature integrity compromises bond strength. Channel deformation or bond weakness was generally more noticeable at substrate edges. In preliminary trials we also explored vacuum plasma, corona and solvent pre-treatment prior to low temperature fusion bonding. From this we found the solvent-assisted approach to offer the greatest potential for uniform and high integrity bonding.

Bond strengths have been evaluated by a number of techniques including crack-opening (Li et al. 2009), shear (Ng et al. 2008) and tensile testing (Brown et al. 2006). We observed a maximum bond strength of 3.8 MPa for double-sided solvent exposure for 12 min via tensile testing. For single-sided bonding, the maximum bond strength was lower at 2.9 MPa. Literature reports indicate much weaker bonds using similar tensile testing for non-solvent techniques such as VUV/O_3 (< 1 MPa), O_2 plasma (< 1.5 MPa) (Brown et al. 2006; Shinohara et al. 2011; Li et al. 2009). A similar conclusion results when shear bond strengths are compared. Solvent assisted bonding has demonstrated much greater achievable bond strengths from 0.5 - 15 MPa (Brown et al. 2006; Rahbar et al. 2010; Ogilvie et al. 2010; Umbrecht et al. 2009) when the solvent is applied to the PMMA surface in liquid form via droplet application or sample immersion. In the latter case, the use of thermally activated solvents (e.g. IPA) is necessary in order to prevent rapid dissolution of patterned features (Ng et al. 2008) while the droplet application method is unsuitable for high resolution patterned substrates. Solvent vapour exposure has been reported as a method of channel smoothing (Ogilvie et al. 2010) and in the latter case, Ogilvie et al. (2010) also report vapour solvent assisted bonding although the bond strength values cannot be compared to ours. They did however observe a narrow process time window (< 40 s) between insufficient exposure time (bond failure) and over-exposure (channel collapse). We did not observe any channel collapse, across the process window. The bond pressure leads to a channel height reduction of ~13% for double-sided and 13% - 20% for single-sided bonding, with exposure of the blank substrate resulting in the greater channel deformation. Preliminary flow tests show that long channel flow resistance variability is less than 2% between channels, implying little variation in average channel height across the substrate. Bonding induced channel height reduction can therefore be accounted for in the device design.

$CHCl_3$ has one of the closest Hildebrand solubility parameters (Brandrup et al. 1975) to that of PMMA, ensuring maximum solvent capability and leading to rapid feature dissolution on contact. However in a vapour process, its high vapour pressure and solvent capability offers optimal exposure times for process control. The permeant ($CHCl_3$) – polymer interaction is thought to lead to a swollen layer and the

possibility of channel distortion upon pressure (Wallow et al. 2007), depending on the extent of the permeation, which in our case is ~60 µm. However subsequent heating to the reduced T_g of the permeated (PMMA + $CHCl_3$) surface (~80 ºC) causes vapour loss, improves the channel profile resilience while permitting interaction with the permeant layer for bonding. Surface softness versus vapour removal become the adjustable parameters for optimising bond strength against distortion and possible solvent induced fatigue. Raman results provide an indication of the changes in $CHCl_3$ after many hours under vacuum or in air and at high temperature. This implies that sensitivity to practical transfer times (minute) during normal processing is not critical. Nevertheless it is clear that irrespective of treatment times and temperature, significant $CHCl_3$ remains at the bond interface. Reduction of the $CHCl_3$ content may be advantageous to limit channel distortion or to limit the exposure, during device operation, of the analyte to outgassed $CHCl_3$ in the region above the channel. While for double-sided bonding, it appears possible given the flat bond strength characteristic, Fig. 2, the single-sided case appears much more sensitive to exposure time and would require further optimisation.

Of course, the practical requirements for bond strength in actual devices are unknown. For single-layer structures, the pressure-leak tests show no leakage up to 10 bar providing strong evidence that the bonding is uniformly robust over a large area. This test showed also that for high resolution patterns, where the bond contact area between the channels is very limited, that no local leakage occurred. This provides valuable evidence that results from tensile tests on small unpatterned samples remain relevant for large device-equivalent pieces. It was also shown that the inclusion of metal tracks within the bond interface did not affect performance. This is an important consideration for conductivity-based elements and electrical connections within channels. Multi-layer bonding however highlighted issues with significant reduction in bond strength when channels were misaligned i.e. when the bond face on layer A was not fully supported by the equivalent bond face on layer C, despite the intervening blank substrate B. The bond strength shows a clear linear dependence on the support area, Fig. 4 (b). The relatively low stiffness of the PMMA sheets at the bonding temperature (80 ºC) would lead to a non-uniform load transfer, and the bonding pressure experienced by patterns on A would not be uniform, leading to bond strength reduction. This is highlighted particularly when two sheets (A) are oriented at 90º and the overlapping area of support is a minimum. The resulting bond strength is reduced by over 90%. Failure only occurs for A surfaces (surface with less total surface area), despite the fact that the average bond pressure experienced by such a surface is 25% higher; the effect of non-uniform load transfer therefore plays a significant role in the resulting bond strength. This is a critical factor in channel layout design, substrate alignment accuracy during fabrication and realistic testing for bond – strength in actual devices. Multi-layer channel layout design therefore becomes a parameter within the device fabrication process. Single sided exposure bonding is favoured for multi-layer stacks since the whole stack can be bonded in a single step which helps preserve channel alignment between layers. For double-sided exposure bonding with high resolution patterns, we noted bond weakness when the wall between channels was reduced to 100 µm whereas single-sided exposure of the unpatterned side retained the bond strength. At pressures below failure, no bulging of the wall was observed and failure was a catastrophic event at the bond interface. The penetration of $CHCl_3$ on all sides of a thin wall can be expected to result in greatly increased pliability and possible sagging, for dimensions less than twice the penetration depth. This will be important for multi-channel architectures and will impact on the design of serpentine or similar structures. With single-layer devices, the exposure of the unpatterned substrate is a viable option to avoid such problems but in multi-layer devices, exposure of the patterned pieces is required for alignment.

Conclusions

Solvent vapour-assisted thermal fusion bonding of PMMA was investigated, using $CHCl_3$ vapour to soften the surface of the thermoplastic prior to bonding, while leaving the bulk unaffected. This process, in principle, allows for bonding well below the T_g of PMMA (~ 105°C), with reduced channel and bulk distortion, compared to thermal-only bonding at or above the T_g. Optimisation of the pre-treatment time, at 4 mm height in a closed vessel, by measuring subsequent bond strengths after vacuum anneal at 80°C, suggest an overall best vapour exposure time of 12 min. Peak tensile and shear bond strengths greater than 3 MPa were achieved for a typical channel depth reduction of 25 µm, or 12.5% for a channel depth of 200 µm. Bonding of multiple layers containing high resolution microfluidic channels was investigated for single and double sided vapour treatments at the optimum pre-treatment of 12 min duration. Single-sided vapour exposure is shown to be suitable for multilayer bonding with better interlayer alignment than double-sided vapour pre-treatments, as the layers slide laterally with respect to each other more easily

for the latter. However, the single-sided vapour process gives more channel depth loss, as a result of pressing a soft surface onto a hard surface. It also gives a weaker bond, presumably because the $CHCl_3$ molecules from the treated side do not penetrate as deeply into the untreated PMMA in the opposing piece, so that polymer chain mixing across the bond interface is reduced compared to the double-sided process. Bond strength reduction is from 20% (lid exposure) to 13% (channel exposure) and 14% (double-sided exposure). Nevertheless, leak and burst tests demonstrate bond integrity up to at least 10 bar channel pressure over the full substrate area of 100 mm x 100 mm. Bonding channels over planar Au metal tracks of 50 nm thickness was shown to create no areas of bond weakness in the vicinity of the electrode/channel crossing points. The vertical wall integrity between channels was found to be compromised by solvent permeation for wall thicknesses of 100 mm which has implications for high resolution serpentine structures. The bond strength decreased linearly to over 90% for multi-layer substrates with increasing misaligned patterns on each layer, despite the presence of an intermediate blank substrate. We have demonstrated that single or double sided vapour pre-treatments of PMMA gives strong uniform bonds which have the potential to permit fabrication of multilayer microfluidic devices containing channel-crossing thin film electrodes. The bond strengths achieved, and the leak and burst pressure of > 10 bar demonstrated, suggest that devices fabricated by the techniques employed will be suitable for lab-on-chip deployment in harsh environmental conditions for applications such as deep ocean profiling.

Acknowledgements
The authors would like to acknowledge the funding support from the Department of Employment & Learning, N. Ireland (US-IRL 013), Science Foundation Ireland (09/US/I1758), and National Science Foundation (US) (NSF 0961250). We would also like to acknowledge Todd Martz and Phil Bresnahan of Scripps Institute of Oceanography for their support and encouragement through fruitful discussions on device design, test and deployment.

Notes and references
[a] School of Mechanical and Aerospace Engineering, Queen's University Belfast, Belfast BT9 5AH, United Kingdom. Email: d.sun@qub.ac.uk; Fax: +44 28 90974148; Tel: +44 28 90974701
[b] Nanotechnology and Integrated Bio-Engineering Centre (NIBEC), University of Ulster, Newtownabbey BT37 0QB, United Kingdom
[c] School of Electronics, Electrical Engineering and Computer Science, Queen's University Belfast, Belfast BT9 5AH, United Kingdom
[d] School of Physics and Ryan Institute, National University of Ireland, Galway, Ireland

References

Alexandra M, Tsalogou NM, Mowlem MC, Keevil CW, Connelly DP (2013), Hyperbaric biofilms on engineering surfaces formed in the deep sea. Biofouling: J Bioadhesion Biofilm Res 29: 1029-1042.

Awaja F, McKenzie DR, Zhang S, James N(2011) Free radicals created by plasmas cause autohesive bonding in polymers. Appl Phys Lett 98: 211504- 211504-3.

Baby A, Mahony, CMO, Lemoine P, Maguire PD (2011), Acetylene–argon plasmas measured at an rf-biased substrate electrode for diamond-like carbon deposition: II. Ion energy distributions. Plasma Sources Sci. Technol. 20: 015004.

Brandrup J, Immergut EH (1975), Polymer Handbook, 4th edition, Wiley, New York.

Bridle H, Miller B, Desmulliez MPY (2014) Application of microfluidics in waterborne pathogen monitoring: A review. Water Res 55:256-271.

Brown L, Koerner T, Horton JH, Oleschuk RD (2006) Fabrication and characterization of poly(methylmethacrylate) microfluidic devices bonded using surface modifications and solvents. Lab Chip 6: 66-73.

Byrne RH (2014) Measuring Ocean Acidification: New Technology for a New Era of Ocean Chemistry. Environ Sci Tech: 48:5352-5360.

Callaghan AH, Ward B, Vialard J (2014), Influence of surface forcing on near-surface and mixing layer turbulence in the tropical Indian Ocean. Deep-sea Res Pt I 94: 107-123.

De Marco C, Eaton S, Martinez-Vazquez R, Rampini S, Cerullo G, Levi M, Turri S, Osellame R (2013) Solvent vapor treatment controls surface wettability in PMMA femtosecond-laser-ablated microchannels. Microfluid Nanofluid 14: 171 -176.

Ducrée J. (2013), Integration of functional materials and surface modification for polymeric microfluidic systems. J Micromech Microeng 23: 033001.

Field CB, Barros VR, Dokken DJ, Mach KJ, Mastrandrea MD, Bilir TE, Chatterjee M, Ebi KL, Estrada YO, Genova RC, Girma B,. Kissel ES, Levy AN, MacCracken S, Mastrandrea PR, and White LL (eds.) (2014), IPCC Summary for policymakers. In: Climate Change 2014: Impacts,Adaptation, and Vulnerability. Part A: Global and Sectoral Aspects, Contribution of Working Group II to the Fifth Assessment Report of the Intergovernmental Panel on Climate, Cambridge, UK and New York, USA.

Hall PO, Aller RC (1992), Rapid, small-volume, flow injection analysis for ΣCO2 and NH+4 in marine and fresh-waters. Limnol Oceanogr 37: 1113-1119.

Herzog G, Moujahid W, Twomey K, Lyons C, Ogurtsov VI (2013) On-chip electrochemical microsystems for measurements of copper and conductivity in artificial seawater. Talanta 116:26 - 32.

http://www.act-us.info/, (accessed Dec 2014).

http://www.argo.ucsd.edu/, (accessed Jun 2014).

http://www.socat.info/about.html, (accessed Dec 2014).

Kettner P, Pelzer RL, Glinsner T, Farrens S, Lee D (2006) New Results on Plasma Activated Bonding of Imprinted Polymer Features for Bio MEMS Applications. J Phys Conf Ser 34: 65 -71.

Legiret FE, Sieben VJ, Woodward E, Malcolm S, Abi KB, Samer, K. Mowlem MC, Connelly DP, Achterberg EP (2013) A high performance microfluidic analyser for phosphate measurements in marine waters using the vanadomolybdate method. Talanta 116: 382-387.

Li JM, Liu C, Liu JS, Xu Z, Wang LD (2009) Multi-layer PMMA microfluidic chips with channel networks for liquid sample operation. J Mat Process Tech 209: 5487-5493.

Li SW, Xu JH, Wang YJ, Lu YC, Luo GS (2009), Low-temperature bonding of poly-(methyl methacrylate) microfluidic devices under an ultrasonic field. J Micromech Microeng 19: 015035.

Lin CH, Chao CH, Lan CW (2007), Low azeotropic solvent for bonding of PMMA microfluidic devices, Sens Actuators B 121: 698-705.

Mills G, Fones G (2012), A review of in situ methods and sensors for monitoring the marine environment. Sensor Rev 32:17-28.

Ng SH, Tjeung RT, Wang ZF, Lu ACW, Rodriguez I, de Rooij, NF (2008,) Thermally activated solvent bonding of polymers. Microsyst Technol 14:753-759.

Ogilvie IRG, Sieben VJ, Cortese B, Mowlem MC, Morgan H (2011), Chemically resistant microfluidic valves from Viton® membranes bonded to COC and PMMA. Lab Chip 11: 2455 -2459.

Ogilvie IRG, Sieben VJ, Floquet CFA, Zmijan R, Mowlem MC, Morgan H (2010) Reduction of surface roughness for optical quality microfluidic devices in PMMA and COC. J Micromech Microeng 20: 065016.

Plant JN, Johnson KS, Needoba JA, Coletti LJ (2009) NH4-Digiscan: an in situ and laboratory ammonium analyzer for estuarine, coastal, and shelf waters. Limnol Oceanogr Meth 7: 1 44-156.

Provin C, Fukuba T, Okamura K, Fujii T (2013) An Integrated Microfluidic System for Manganese Anomaly Detection Based on Chemiluminescence: Description and Practical Use to Discover Hydrothermal Plumes Near the Okinawa Trough. IEEE J Oceanic Eng 38:178-185.

Rahbar M, Chhina S, Sameoto D, Parameswaran M (2010) Microwave-induced, thermally assisted solvent bonding for low-cost PMMA microfluidic devices. J Micromech Microeng 20: 015026.

Rérolle VM, Floquet CF, Harris AJ, Mowlem MC, Bellerby RR, Achterberg EP(2013) Development of a colorimetric microfluidic pH sensor for autonomous seawater measurements. Anal Chim Acta 786:124 – 131.

Rothschild WG, Rosasco GJ, Livingston RC (1975) Dynamics of molecular reorientational motion and vibrational relaxation in liquids, Chloroform. J Chem Phys 62: 1253 -1268.

Rusconi R, Garren M Stocker R (2014) Microfluidics Expanding the Frontiers of Microbial Ecology. Annu Rev Biophys 43: 65-91.

Sackmann EK, Fulton AL, Beebe DJ (2014) The present and future role of microfluidics in biomedical research. Nature 507:181 -189.

Shao P, van Kan JA, Wang L, Ansari K, Bettol AA, Watt F (2006), Fabrication of enclosed nanochannels in poly(methylmethacrylate) using proton beam writing and thermal bonding, App Phys Lett 88: 093515.

Seymour JR, Simó R, Ahmed T, Stocker R (2010) Chemoattraction to dimethylsulfoniopropionate throughout the marine microbial food web, Science 329: 342-345.

Shinohara, H, Kasahara T, Shoji S, Mizuno J (2011) Studies on low-temperature direct bonding of VUV/O3-, VUV- and O2 plasma-pre-treated poly-methylmethacrylate. J Micromech Microeng 21: 085028.

Sutherland G, Reverdin G, Marié L, Ward B (2014) Mixed and mixing layer depths in the ocean surface boundary layer under conditions of diurnal stratification. Geophys Res Lett 41: 8469 -8476.

Sutherland G, Ward B, Christensen KH (2013) Wave-turbulence scaling in the ocean mixed layer. Ocean Sci 9: 597-608.

Temiz Y, Lovchik RD, Kaigala GV, Delamarche E (2015) Lab-on-a-chip devices: How to close and plug the lab? Microelectron Eng 132: 156-175.

Tomazelli C, Wendell K, Cheng CM, de Jesus Carrilho E, Dosil P (2014), Recent advances in low-cost microfluidic platforms for diagnostic applications, Electrophoresis 3 5: 2309-2324.

Tran HH, Wu W, Lee NY (2013) Ethanol and UV-assisted instantaneous bonding of PMMA assemblies and tuning in bonding reversibility. Sens Actuators B 181: 955 -962.

Tsao CW, DeVoe D (2009) Bonding of thermoplastic polymer microfluidics. Microfluid Nanofluid 6: 1 - 16.

Tsao CW, Hromada L, Liu J, Kumar P, DeVoe DL (2007) Low temperature bonding of PMMA and COC microfluidic substrates using UV/ozone surface treatment. Lab Chip 7:499-505.

Uba FI, Hu B, Weerakoon-Ratnayake K, Oliver-Calixte N, Soper SA (2015) High process yield rates of thermoplastic nanofluidic devices using a hybrid thermal assembly technique. Lab Chip 15: 1038 -1 049.

Umbrecht F, Müller D, Gattiker F, Boutry CM, Neuenschwander J, Sennhauser U, Hierold Ch (2009) Solvent assisted bonding of polymethylmethacrylate: Characterization using the response surface methodology. Sens Actuators A 156: 121 -128.

Volpatti LR, Yetisen A K (2014), Commercialization of microfluidic devices. Trends Biotechnol 32: 347- 350.

Wallow TI, Morales AM, Simmons BA, Hunter MC, Krafcik KL, Domeier LA, Sickafoose SM, Patel KD, Gardea A (2007) Low-distortion, high-strength bonding of thermoplastic microfluidic devices employing case-II diffusion-mediated permeant activation. Lab Chip 7: 1825-1831.

Ward B, Fristedt T, Callaghan AH, Sutherland G, Sanchez X, Vialard J, ten Doeschate A, Atmos J (2014) The Air–Sea Interaction Profiler (ASIP): An Autonomous Upwardly Rising Profiler for Microstructure Measurements in the Upper Ocean. Oceanic Tech 31:2246-2267.

Whitesides GM (2006), The origins and the future of microfluidics Nature 442:368 -373.

Xi H, Pascal RW, Chamberlain K, Banks CJ, Mowlem M, Morgan F (2011) High Precision Conductivity and Temperature Sensor System for Ocean Monitoring. IEEE Sens J 11:3246-3252.

Zhang Z, Lou Y, Wang X, Zheng Y, Zhang Y, Wang L (2010), Thermal assisted ultrasonic bonding of multilayer polymer microfluidic devices, J Micromech Microeng 20:015036.